Research Article | Vol. 25, No. 24 | 27 Nov 2017 | OPTICS EXPRESS 29896
Optics EXPRESS

Sensitive refractive index sensor based on an assembly-free fiber multi-mode interferometer fabricated by femtosecond laser

PENGCHENG CHEN, XUEWEN SHU,* FANGCHENG SHEN, AND HAORAN CAO

Wuhan National Laboratory for Optoelectronics & School of Optical and Electronic Information, Huazhong University of Science and Technology, Wuhan 430074, China
xshu@hust.edu.cn

Abstract: We propose and demonstrate a highly sensitive refractive index (RI) sensor based on a novel fiber-optic multi-mode interferometer (MMI), which is formed with a femtosecond-laser-induced in-core negative refractive index modified line in a standard single mode fiber. The proposed MMI structure is directly written with femtosecond laser in one step, which removes the splicing process needed in conventional MMI fabrication and also significantly improves the robustness. This device exhibits a high sensitivity to surrounding refractive index, with a maximum sensitivity up to 10675.9 nm/RIU at the RI range of 1.4484-1.4513. The distinct advantages of high sensitivity, compact, robust and assembly-free all-fiber structure make it attractive for real physical, chemical and biological sensing.

OCIS codes: (060.2340) Fiber optics components; (060.2370) Fiber optics sensors; (230.1150) All-optical devices.

References and links

1. W. Liang, Y. Huang, Y. Xu, R. K. Lee, and A. Yariv, "Highly sensitive fiber Bragg grating refractive index sensors," Appl. Phys. Lett. **86**(15), 151122 (2005).
2. N. Chen, B. Yun, and Y. Cui, "Cladding mode resonances of etch-eroded fiber Bragg grating for ambient refractive index sensing," Appl. Phys. Lett. **88**(13), 133902 (2006).
3. S. C. Warren-Smith and T. M. Monro, "Exposed core microstructured optical fiber Bragg gratings: refractive index sensing," Opt. Express **22**(2), 1480–1489 (2014).
4. V. Bhatia and A. M. Vengsarkar, "Optical fiber long-period grating sensors," Opt. Lett. **21**(9), 692–694 (1996).
5. S. Xuewen, Z. Lin, and I. Bennion, "Sensitivity characteristics of long-period fiber gratings," J. Lightwave Technol. **20**(2), 255–266 (2002).
6. S. W. James and R. P. Tatam, "Optical fibre long-period grating sensors: Characteristics and application," Meas. Sci. Technol. **14**(5), R49–R61 (2003).
7. F. De-Jun, Z. Mao-Sen, G. Liu, L. Xi-Lu, and J. Dong-Fang, "D-Shaped Plastic Optical Fiber Sensor for Testing Refractive Index," IEEE Sens. J. **14**(5), 1673–1676 (2014).
8. H. H. Qazi, A. B. b. Mohammad, H. Ahmad, M. Z. Zulkifli, and S. W. Harun, "Single-mode D-shaped optical fiber sensor for the refractive index monitoring of liquid," J. Mod. Opt. **63**(8), 750–755 (2015).
9. C. H. Chen, T. C. Tsao, J. L. Tang, and W. T. Wu, "A multi-D-shaped optical fiber for refractive index sensing," Sensors (Basel) **10**(5), 4794–4804 (2010).
10. C. H. Chen, J. L. Tang, and W. Wu, "Novel Multi-D-Shape Fiber Optic Biosensor," in *Proceedings of the 5th International Symposium on Machinery and Mechatronics for Agriculture and Biosystems Engineering, Fukuoka, Japan*, 2010, 25–28.
11. Y. Y. Shevchenko and J. Albert, "Plasmon resonances in gold-coated tilted fiber Bragg gratings," Opt. Lett. **32**(3), 211–213 (2007).
12. P. Bhatia and B. D. Gupta, "Surface-plasmon-resonance-based fiber-optic refractive index sensor: sensitivity enhancement," Appl. Opt. **50**(14), 2032–2036 (2011).
13. L. Li, L. Xia, Z. Xie, and D. Liu, "All-fiber Mach-Zehnder interferometers for sensing applications," Opt. Express **20**(10), 11109–11120 (2012).
14. M. Han, F. Guo, and Y. Lu, "Optical fiber refractometer based on cladding-mode Bragg grating," Opt. Lett. **35**(3), 399–401 (2010).
15. K. Mileńko, D. J. Hu, P. P. Shum, T. Zhang, J. L. Lim, Y. Wang, T. R. Woliński, H. Wei, and W. Tong, "Photonic crystal fiber tip interferometer for refractive index sensing," Opt. Lett. **37**(8), 1373–1375 (2012).
16. Z. Tian, S. S. H. Yam, and H.-P. Loock, "Refractive index sensor based on an abrupt taper Michelson interferometer in a single-mode fiber," Opt. Lett. **33**(10), 1105–1107 (2008).
17. R. Yang, Y. S. Yu, Y. Xue, C. Chen, Q. D. Chen, and H. B. Sun, "Single S-tapered fiber Mach-Zehnder interferometers," Opt. Lett. **36**(23), 4482–4484 (2011).

#307229 https://doi.org/10.1364/OE.25.029896
Journal © 2017 Received 15 Sep 2017; accepted 30 Oct 2017; published 15 Nov 2017

Optics EXPRESS

18. Q. Wang and G. Farrell, "All-fiber multimode-interference-based refractometer sensor: proposal and design," Opt. Lett. **31**(3), 317–319 (2006).
19. Z. B. Liu, Z. Tan, B. Yin, Y. Bai, and S. Jian, "Refractive index sensing characterization of a singlemode-claddingless-singlemode fiber structure based fiber ring cavity laser," Opt. Express **22**(5), 5037–5042 (2014).
20. R. Jha, J. Villatoro, G. Badenes, and V. Pruneri, "Refractometry based on a photonic crystal fiber interferometer," Opt. Lett. **34**(5), 617–619 (2009).
21. R. Jha, J. Villatoro, and G. a. Badenes, "Ultrastable in reflection photonic crystal fiber modal interferometer for accurate refractive index sensing," Appl. Phys. Lett. **93**(19), 191106 (2008).
22. L. Xu, Y. Li, and B. Li, "Nonadiabatic fiber taper-based Mach-Zehnder interferometer for refractive index sensing," Appl. Phys. Lett. **101**(15), 153510 (2012).
23. P. Lu, L. Men, K. Sooley, and Q. Chen, "Tapered fiber Mach–Zehnder interferometer for simultaneous measurement of refractive index and temperature," Appl. Phys. Lett. **94**(13), 131110 (2009).
24. W. B. Ji, H. H. Liu, S. C. Tjin, K. K. Chow, and A. Lim, "Ultrahigh Sensitivity Refractive Index Sensor Based on Optical Microfiber," IEEE Photonics Technol. Lett. **24**(20), 1872–1874 (2012).
25. P. Wang, G. Brambilla, M. Ding, Y. Semenova, Q. Wu, and G. Farrell, "High-sensitivity, evanescent field refractometric sensor based on a tapered, multimode fiber interference," Opt. Lett. **36**(12), 2233–2235 (2011).
26. Q. Wu, Y. Semenova, P. Wang, and G. Farrell, "High sensitivity SMS fiber structure based refractometer--analysis and experiment," Opt. Express **19**(9), 7937–7944 (2011).
27. W. Watanabe, T. Asano, K. Yamada, K. Itoh, and J. Nishii, "Wavelength division with three-dimensional couplers fabricated by filamentation of femtosecond laser pulses," Opt. Lett. **28**(24), 2491–2493 (2003).
28. E. Bricchi, B. G. Klappauf, and P. G. Kazansky, "Form birefringence and negative index change created by femtosecond direct writing in transparent materials," Opt. Lett. **29**(1), 119–121 (2004).
29. J. W. Silverstone, S. McFarlane, C. P. Manchee, and A. Meldrum, "Ultimate resolution for refractometric sensing with whispering gallery mode microcavities," Opt. Express **20**(8), 8284–8295 (2012).

1. Introduction

All-fiber refractive index (RI) sensors are important in chemical and biotechnology applications for a range of superior advantages, such as high sensitivity, low cost, compact size, immunity to electron-magnetic interference and usage in harsh environments. In the past few years, a number of all-fiber RI sensors have been developed, including fiber Bragg grating (FBG) [1–3], long-period grating (LPG) [4–6], D-shaped optical fiber [7–10], microstructure fiber [3], surface plasmon resonance (SPR) [11, 12], cascaded/hybrid configuration [13, 14] and a variety of fiber interferometers [15–17]. Among them, multimode interferometer (MMI)-based RI optical sensors have attracted great attention recently owing to their distinct advantages of ease of fabrication and low cost. The MMI-based sensors are usually fabricated by splicing special fibers, such as multimode fiber (MMF) [18], no core fiber (NCF) [19], photonic crystal fiber (PCF) [20, 21], or using fiber taper technology [22–24]. However, special fibers are expensive and need special splicing program to assemble the individual fibers together. Besides, for some special fiber based MMI structures, part of fiber cladding needs to be removed or thinned [25, 26] to obtain high RI sensitivity, which usually needs additional chemical etching process or fiber tapering technology. And the thinned/tapered fiber inherently has a bad mechanical strength and short service life.

Previously, it has been reported that multimode interference waveguide in bulk glass can be fabricated by a femtosecond laser (fs-laser) [27]. However, the device is not compatible with optical communication systems since it requires complex arrangements of lens to shape and couple the light beams, and the operating wavelength is beyond the communication wavelength. Optical fiber could be a perfect platform to fabricate MMI structures due to its inherent properties of compact size, low cost and naturally compatible with existing optical communication system.

In this paper, we propose and experimentally demonstrate a novel assembly-free fiber inline MMI in a common telecommunication single mode fiber (SMF). The device is based on an in-core negative refractive index modification line (NRIML), fabricated by one-step femtosecond laser direct writing without using any patterned masking or post-processing. Compared with assembly-based MMI and tapered MMI, our proposed NRIML-based MMI has the advantages of simple structure, assembly-free, ease of fabrication, good robustness

Optics EXPRESS

and low cost. As a RI sensor, a maximum sensitivity of 10675.9 nm/RIU is achieved in the RI range of 1.4484-1.4513.

2. Schematic and fabrication of the MMI

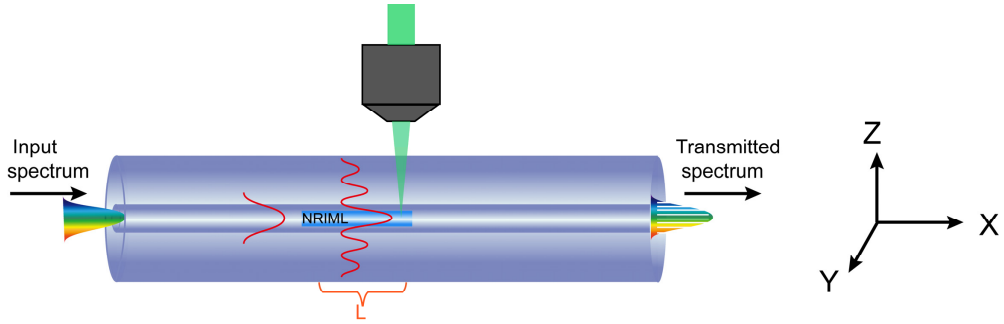

Fig. 1. Schematic diagram of the assembly-free MMI.

The schematic configuration of the proposed MMI is illustrated in Fig. 1. The MMI structure comprises a section of in-core NRIML, which can be obtained by direct fs-laser writing in the SMF. Usually, to obtain negative index change, relatively high pulse energy for fs-laser writing has to be used [28]. As is known to all, light trends to concentrate on the media with a larger refractive index. Generally, the refractive index of the fiber core is larger than the cladding, which makes the light field tightly confined in the core. However, due to the inducing of the NRIML, the average refractive index of the fiber core decreases. When the refractive index of the fiber core is decreased to be smaller than that of the cladding, the light energy will widely spread into the cladding in the NRIML zone. Thus, multimode interference occurs.

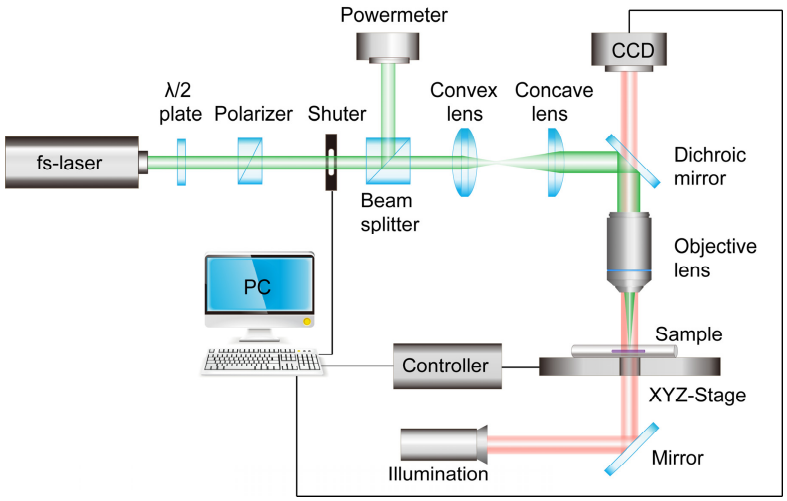

Fig. 2. Experimental setup for direct femtosecond laser writing NRIML.

Figure 2 shows the schematic of the fs-laser direct writing system used for NRIML fabrication. The repetition rate, central wavelength, and pulse width of the fs laser (Spectra-Physics, Spirit 1040-8-SHG) are 200 kHz, 520 nm, and 350 fs, respectively. The laser power was adjusted by a $\lambda/2$ plate in combination with a polarizer. A mechanical shutter was employed to control the exposure time. To monitor the stability of the laser power during fabrication, a beam splitter was utilized to split the input laser beam into two with a fixed intensity ratio. One of the split beam was monitored by a power meter, and the other beam

Optics EXPRESS

passed through a convex and concave lens to produce a high-quality collimated beam. The laser beam was then directed into a microscope objective (Olympus UMPLFL 40X) with a numerical aperture (NA) of 0.65 and focused into the core of a SMF (Yangtze Optical Fiber and Cable Company Ltd.) with a core/cladding diameter of 8.3/125μm. The fiber was mounted on a computer-controlled XYZ translation stage (Newport, Inc.) with a resolution of 0.02 μm. An online monitoring CCD system was used to monitor the sample morphology during the direct writing process. The actual laser energy used for the fabrication was approximately 3μJ/pulse.

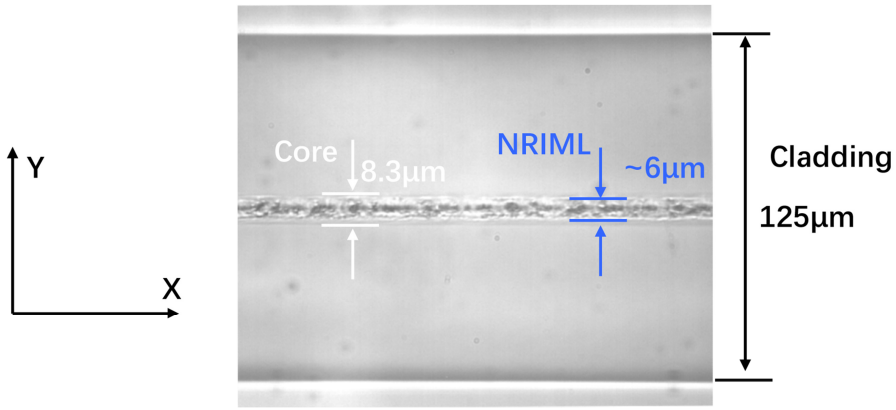

Fig. 3. Microscope image of the in-fiber-core NRIML sample.

3. Principle and spectra characteristics

During the fabrication of the device, the transmission spectrum was real-time monitored by a spectral monitoring system, which included a super-continuum white light source (YSL Super-continuum Source SC-5), and an optical spectrum analyzer (OSA, YOKOGAWA AQ6370C). The fabrication process of the proposed MMI was quite straightforward and involved only one step. When the center of the fiber core was correctly aligned to the focus point of the fs-laser (z-direction), a NRIML can be directly written by scanning the fiber along its core axis (x-direction). The scanning speed used in our experiment was 200 μm/s. Figure 3 shows the microscope image of a small part of the NRIML structure fabricated in the fiber core.

After propagation along the NRIML, the phase difference (φ) of the fundamental mode and any higher-order mode involved in the interference can be written as

$$\varphi = \frac{2\pi \Delta n_{eff} L}{\lambda} \tag{1}$$

Here Δn_{eff} is the effective refractive index difference of the two interference modes, L is the length of the NRIML and λ is the wavelength in vacuum. When $\varphi = (2m+1)\pi$, the wavelength of the interference dip (λ_m) will appear at

$$\lambda_m = \frac{2\pi \Delta n_{eff} L}{2m+1}, \quad m = 1, 2, 3 \ldots \tag{2}$$

When the surrounding refractive index changes, the effective refractive index of the higher order modes usually also changes, which will result in the shift of the wavelength of the interference dip. Therefore, one could measure the surrounding refractive index by

Optics EXPRESS

monitoring the wavelength shift of the spectrum. Based on Eq. (2), the wavelength spacing ($\Delta\lambda$) can be calculated as

$$\Delta\lambda \approx \frac{\lambda^2}{\Delta n_{eff} L} \tag{3}$$

According to Eq. (3), $\Delta\lambda$ decreases with the length of NRIML increasing.

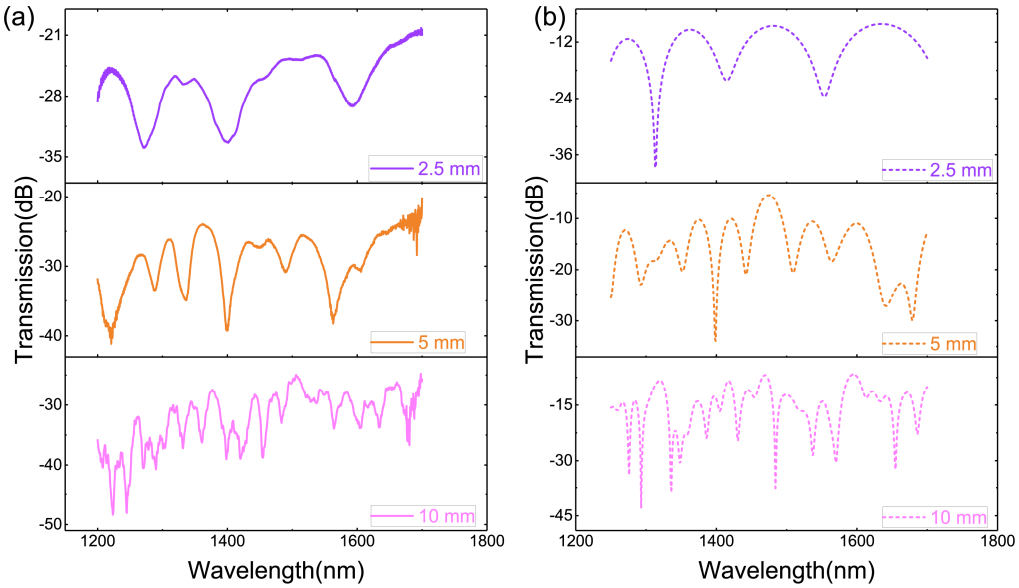

Fig. 4. (a) Measured transmission spectra of the MMIs with different NRIML lengths. (b) The corresponding simulated transmission spectra of the MMIs with different NRIML lengths.

The measured transmission of the MMI with different NRIML length of 2.5 mm, 5 mm and 10 mm are shown in Fig. 4(a), from which we can see that the longer NRIML length corresponds to the larger insertion loss. Because when the NRIML becomes longer, the light suffers more scattering and diffraction. It is also evident that with the increase of the NRIML length, the wavelength spacing between two adjacent interference fringes dips decreases, which is good accord with Eq. (3).

Optics EXPRESS

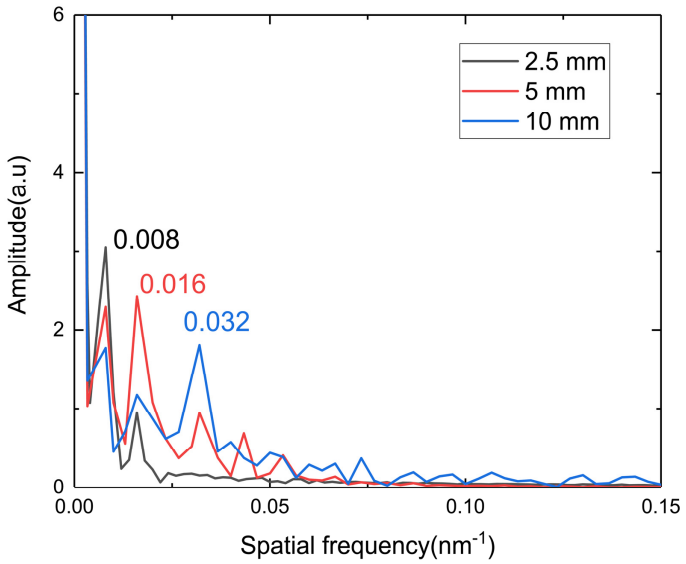

Fig. 5. Spatial frequency of the MMIs with different lengths.

In order to analyze the number and the power distribution of the interference modes, the experimental spectra in Fig. 4(a) are taken fast Fourier transform (FFT) to obtain the spatial frequency spectra, as shown in Fig. 5. It is seen in Fig. 5 that there are two or three dominant peaks in the spatial spectra, which means two or three pairs of dominant modes are mainly associated with the interference spectra. The dominant maximum frequency are located at ~0.008, 0.016 and 0.032 nm^{-1} for MMI length of 2.5, 5 and 10 mm, respectively, which are well in accord with Fig. 4(a) and Eq. (3).

4. Refractive index sensing, simulation and discussion

To characterize the RI response of the structure, one sample with 5 mm NRIML length was immersed in a series of sucrose solutions with different concentrations and the corresponding transmission spectra were recorded by the OSA. When the surrounding RI was increased from 1.3333 to 1.4513, the transmission spectrum evolution of the sample was shown in Fig. 6. It can be clearly seen in Fig. 6 that, with the increase of the RI, the dip wavelengths in the transmission spectra had a significant monotonic red shift, and the wavelength change rate became faster with the RI increasing. The wavelength shifts of the dips A, B and C were chosen to be traced when the MMI was immersed into different solutions.

Optics EXPRESS

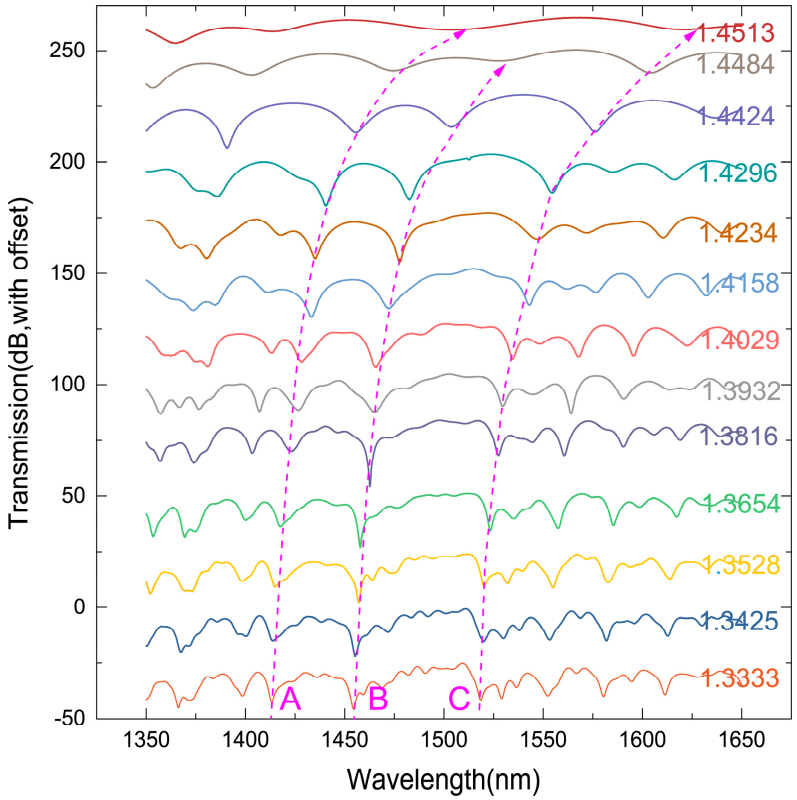

Fig. 6. Transmission spectra evolution of the MMI under different surroundings RI.

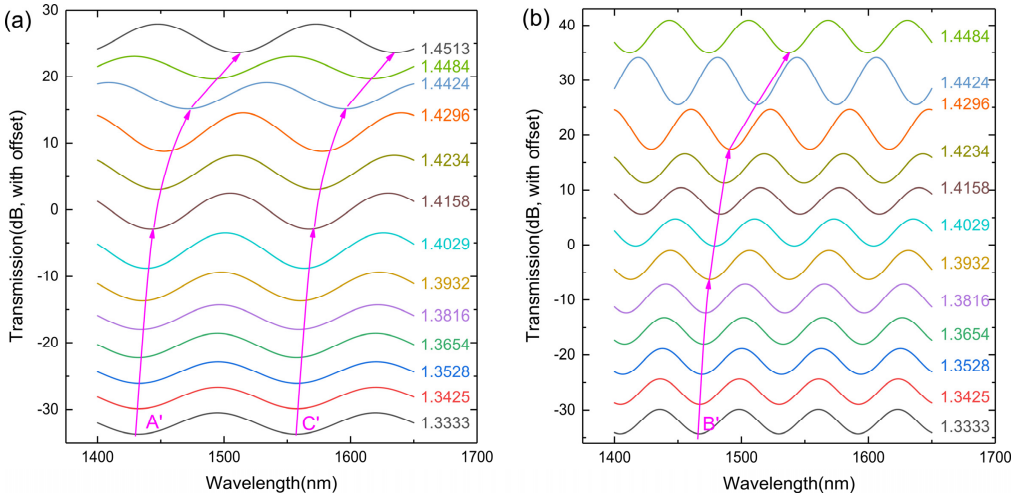

Fig. 7. The lower-order (a) and higher-order (b) dominant sinusoidal component of the DFT spectra evolution under different surrounding RI.

Figure 5 and 6 show that there are multiple pairs of modes contributing to the complex interference spectrum and the spectral overlapping will likely occur between these mode interferences, so the method of directly tracking individual dips might not be very precise. Discrete Fourier transform (DFT) method [29] has been demonstrated as a good technique to solve such a problem. For the measured 5-mm-long sensor, the dominant frequencies of the two pairs of interference modes are located at 0.008 and 0.016 nm^{-1}, respectively. Two band-

Optics EXPRESS

pass DFT filters with frequency range in 0.006-0.01 and 0.014-0.018nm^{-1}, respectively, were chosen to extract each individual mode pair at different surrounding RI. The DFT spectrum evolutions are shown in Fig. 7(a) and 7(b), where sinusoidal components are clearly seen. Dips A', B' and C' in Fig. 7 corresponding to the Dips A, B and C in Fig. 6, respectively. Obviously, the Dips A' and C' stem from the same low order mode pairs and the Dip B' stems from a higher order mode pair.

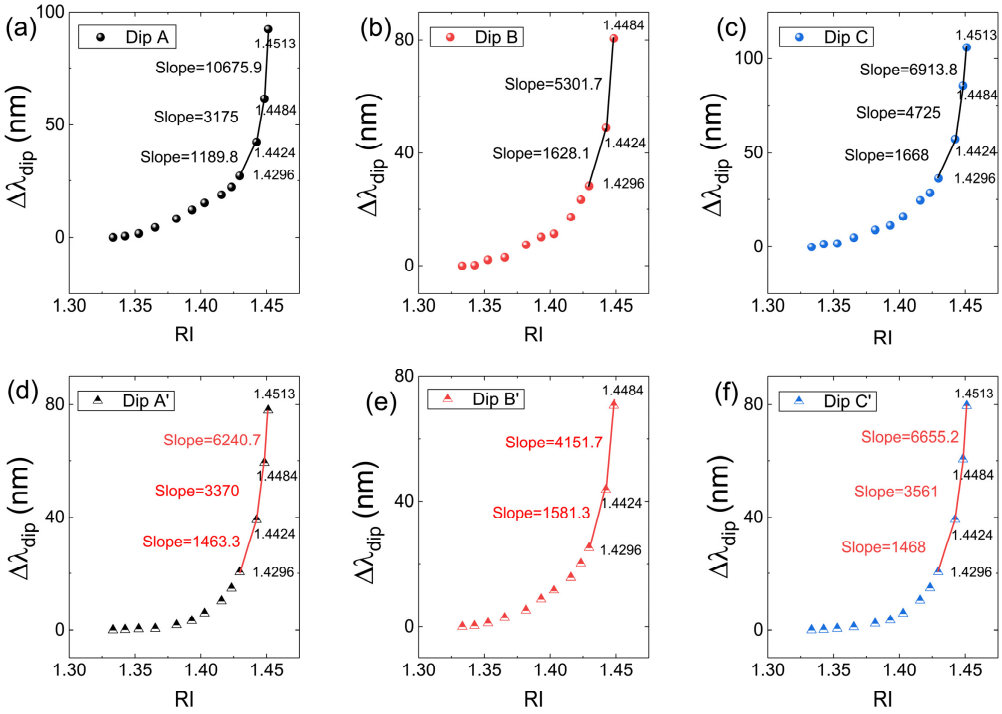

Fig. 8. (a)-(c) Wavelength shift of the Dips A, B and C at different RI solutions (d)-(f) Wavelength shift of Dips A', B' and C' at different RI.

For comparison, the wavelength shifts of measured MMI dips obtained by direct spectral tracking and extracted by the DFT method are shown in Fig. 8. The wavelength shifts of the selected Dips A, B and C at different surrounding RI using direct spectral tracking are shown in Figs. 8(a)-8(c), where the maximum sensitivities of 10675.9, 5301.7 and 6913.8 nm/RIU are achieved in the RI range of 1.4484-1.4513, 1.4424-1.4484 and 1.4484-1.4513, respectively. Figures 8(d)-8(f) show the wavelength shifts of the selected Dips A', B' and C' obtained with the DFT method, where the maximum sensitivities of 6240.7, 4151.7 and 6655.2 nm/RIU are achieved in the RI range of 1.4484-1.4513, 1.4424-1.4484 and 1.4484-1.4513, respectively. Dips A' and C' stem from the same lower interference modes pair (frequency~0.008 nm^{-1}), while Dip B' stems from a higher modes pair (frequency~0.016 nm^{-1}). Compared to Dip B', Dips A' and C' can work in a higher RI region (1.4484-1.4513) as the higher order interference mode (Dip B') will disappear first with the RI increasing. Within the same RI range, the sensitivity of Dip B' is larger than Dips A' and C'(e.g., in the RI range of 1.4296-1.4484), which is reasonable since the Dip B' belongs to a higher order mode interference. Without the DFT processing, one cannot find this fact since Figs. 8(a)-8(c) do not shown this.

Optics EXPRESS

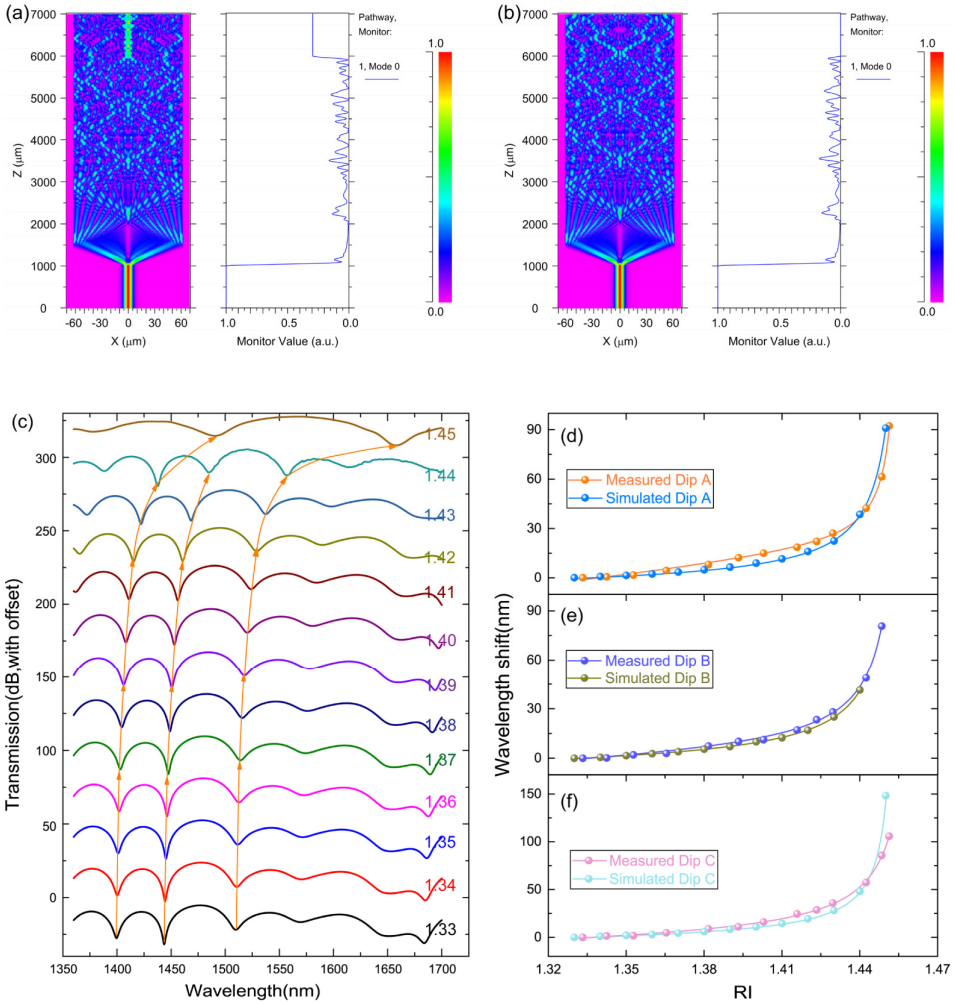

Fig. 9. (a) and (b) The simulated field distribution of the light propagating along the MMI with 5 mm NRIML length at input wavelength of about 1469nm and 1435nm, respectively. (c) Transmission spectra of the MMI with different surrounding RI calculated by BPM. (d)-(f) Simulated and measured the wavelength shifts of the Dips A, B and C with different RI.

The beam propagation method (BPM) is utilized to analyze the property of the proposed MMI. In the simulation, the length and the width of NRIML are 5 mm and 5.6 μm, respectively. The refractive indices of the fiber core and the cladding are assumed to be 1.462 and 1.455, respectively, while the RI modification in the NRIML zone is set to be −0.013. Figure 9(a) and (b) give the simulated normalized field distribution of the light propagating in the MMI structure, where one can clearly see that a large number of cladding modes are excited in the NRIML zone and strong coupling occurs. Figure 9(a) shows the simulation with an input wavelength at about 1469 nm (an interference wavelength peak), where the light has a relatively low loss after the NRIML interference. Figure 9(b) shows the simulation with an input wavelength at about 1435nm (an interference wavelength dip), from which we can see that there is almost no light field in the fiber core after the NRIML interference, but widely spreads into the cladding area. The simulated transmission spectra with NRIML length of 2.5 mm, 5 mm and 10 mm are shown in Fig. 4(b). It is obvious that the simulated wavelength spacing between two adjacent interference fringes dips are consistent with the

Optics EXPRESS

experimental results mentioned above in Fig. 4(a). Figure 9(c) shows the simulated spectral evolution when the surrounding RI varying from 1.33 to 1.45. The simulated and experimental wavelength shifts of the dips at different surrounding RIs are plotted in Fig. 9(d)-9(f), which appear in a good agreement with each other. The small discrepancies between the calculated and experimental results could be due to: (1) the difference between the parameters used in the simulation model and the actual structure (2) the refractive index dispersion, i.e., the refractive index of the sucrose solutions was calibrated using Abbe refractometer (at 589.3 nm), while the sensing experiment carried out in the range of 1400-1600 nm.

5. Conclusion

In conclusion, we have proposed and experimentally demonstrated a novel assembly-free MMI in SMF for RI measurement. The device is simply fabricated by direct fs-laser writing and the whole fabrication process involves only one step. A maximum sensitivity of 10675.9 nm/RIU were achieved in the RI range of 1.4484-1.4513 experimentally. The BPM method is utilized to analyze the property of the proposed MMI, and the simulated sensitivities and their variation trend exhibit high consistency with the experimental results. The proposed MMI sensor possesses the advantages of assembly-free, robustness, compact size, and high RI sensitivity, which make it promising in chemical and biological applications.

Funding

National Natural Science Foundation of China (NSFC) (61775074); National 1000 Young Talents Program, China; 111 Project (No. B07038)